European Journal of Radiology 205 (2026) 113198

Contents lists available at ScienceDirect

European Journal of Radiology

journal homepage: www.elsevier.com/locate/ejrad

Patient dose in HR-pQCT bone scans can be reduced by suitably setting the tube start angle: A proof of concept

Laura Antonia Cerbone [a,b,c], Youfang Lai [d], Xun Jia [d], Steven K. Boyd [e], Giovanni Mettivier [b,c], Paolo Russo [b,c,*]

[a] Scuola Superiore Meridionale, I-80138 Naples, Italy
[b] Dipartimento di Fisica "Ettore Pancini", Università di Napoli Federico II, I-80126 Naples, Italy
[c] Istituto Nazionale di Fisica Nucleare (INFN), Sezione di Napoli, I-80126 Naples, Italy
[d] Department of Radiation Oncology and Molecular Radiation Sciences, Johns Hopkins University, Baltimore MD21287, United States of America
[e] McCaig Institute for Bone and Joint Health, Department of Radiology, Cumming School of Medicine, University of Calgary, Calgary, Alberta T2N 4Z6, Canada

ARTICLE INFO

Keywords:
High-resolution peripheral quantitative computed tomography
Computed tomography dose
Organ dose
Effective dose
Monte Carlo simulation

ABSTRACT

Background: High-resolution peripheral quantitative computed tomography (HR-pQCT) assesses the three-dimensional microarchitecture of distal tibia and radius for bone health evaluation. The effective dose (E) for an HR-pQCT examination is less than 2 μSv. In the standard protocol for patient scans, a default start angular position of the X-ray tube is adopted, in a half-scan geometry. The total half-scan angle (180° + fan angle 22°) determines an uneven distribution of the absorbed dose in the tissues, given the specific anatomy of the bones in the ankle and the wrist. *Purpose* We carried out a Monte Carlo dosimetry study to investigate whether a different choice of the tube start angle could produce scans with lower organ doses and lower E, so reducing the patient radiation risk.
Methods: We performed Monte Carlo simulations at varying tube start angles of the Scanco XtremeCT II scanner, with an angular step of 11°, using a digital twin of the scanner and voxelized phantoms (left and right tibia and radius) derived from a previously available scan of a volunteer subject.
Results: We showed that the tissue-averaged organ dose (for bone, bone marrow, skin, muscle, and fat) depends on the tube start angle, with a pronounced minimum for bone and yellow bone marrow occurring at a specific start angle. At the dose-optimized angle, E shows a minimum, about 10 % lower than for the standard start angle, for the left tibia; for the radius, the dose-optimized protocol allows for a maximum dose sparing of 6.6 %, possibly increasing to over 16 % (tibia scan) if the presence of the limb holder is accounted for. No significant morphologic difference emerged in the CT reconstructions obtained for the standard and dose-optimized protocol.
Conclusions: For patients undergoing HR-pQCT scans the radiation dose, and the related patient risk, could be reduced by selecting the tube start angle.

1. Introduction

High-resolution peripheral quantitative CT (HR-pQCT) [1] is a tomographic technique dedicated to scanning peripheral anatomical sites (wrists, ankles, and knees) used for bone health assessment. HR-pQCT scans allow for measuring the volumetric bone density, via high-resolution 3D images of the internal structure of long bones, the trabecular bone, as well as for evaluating the bone strength via morphologic and finite element analysis [2,3]. HR-pQCT is a relatively recent diagnostic imaging technique for bone-density assessment. It has substantially improved the spatial resolution achievable in peripheral bone imaging, enabling the assessment of bone microarchitecture in the extremities. Although HR-pQCT has primarily been used as a research tool, its use in clinical research and selected clinical applications has increased in recent years. Currently, the XtremeCT II, manufactured by Scanco Medical AG, Switzerland, is the only commercially available HR-pQCT system. The present study therefore focuses on this scanner, which performs tomographic acquisitions using a fan-beam geometry without

* Corresponding author at: Dipartimento di Fisica "Ettore Pancini", Università di Napoli Federico II, Via Cintia 21, I-80126 Napoli, Italy.
E-mail address: paolo.russo3@unina.it (P. Russo).

https://doi.org/10.1016/j.ejrad.2026.113198
Received 3 February 2026; Received in revised form 24 July 2026; Accepted 30 August 2026
Available online 31 August 2026

axial movement of either the patient or the tube-detector system during the acquisition.

Recently, we carried out Monte Carlo (MC) virtual dosimetry for the patient-specific assessment of organ doses and effective dose (E), in HR-pQCT scans of the tibia and radius, using a digital twin of the clinical scanner [4]. The voxelized phantoms for that virtual dosimetry study were derived from patient scan images, via semi-automatic tissue segmentation (bone, bone marrow, skin, muscle, and fat). That first independent virtual dosimetry study – performed via graphics processing unit (GPU)-accelerated MC simulations – determined patient-specific E values of 1.5–2.1 μSv for the distal tibia and radius, slightly lower than the manufacturer's declared E values of 3–5 μSv per scan.

Analysing the dose map within the tissues, we observed a dose gradient in axial slices as high as 1.5 mGy/mm across the bone, which was attributed to the anatomy of the organ and to the partial scan angle used by the HR-pQCT clinical scanner ($\Delta\theta = 202^\circ = 180^\circ + 22^\circ$ *fan angle*). Indeed, the half-scan geometry produces a less uniform dose distribution in the organ than using a full-scan geometry (see Supplementary material). During that study, we hypothesized that by changing the start angle θ_0 of the scan $\left(\theta_0 = \frac{fan\ angle}{2} = -11^\circ\right)$ adopted in the standard scanning protocol (Fig. 1), the organ dose, and the bone dose specifically, might be reduced by a suitable selection of a dose-optimized start angle ($\theta_0 = \theta_0^*$).

We expect that the value of θ_0^* depends on the anatomy of the patient and on the position of the organ in the scanner field of view. While E for an HR-pQCT scan of the tibia or radius is extremely low [4,5] (equivalent to just 11 min of exposure to natural radioactivity background, for an annual E of 2.4 mSv for the population), dose optimization in radiological medical imaging procedures should always be carefully considered, as the second of the three fundamental principles of radiological protection—*verbatim*, "justification, optimisation of protection, and application of dose limits" [6]. This follows the recommendations by the International Commission on Radiological Protection (ICRP), in the continuing process of devoting efforts for optimization through "balancing the benefits and detriments of protective actions to achieve the greatest overall benefit" [6].

Based on the above considerations, we were motivated to explore, via MC simulations, the dependence of the effective dose in HR-pQCT patient scans on the tube start angle, at the same time assessing the quality of the reconstructed CT image for the standard scan protocol ($\theta_0 = -11^\circ$) and the dose-optimized ($\theta_0 = \theta_0^*$) protocol, to determine any corresponding change in image quality. This dosimetric approach is also relevant to repeated HR-pQCT scans, as research studies usually require periodical rescanning of patients or scanning more than one anatomical site, hence multiplying the dose burden to the patients and their corresponding radiation risk [7].

Here, we carried out a MC-based virtual dosimetry study for assessing, in one demonstrative case, the possibility of reducing the effective dose, and quantified this reduction by defining a dose-optimized scanning protocol via a dose reduction strategy implementing a new setting of the X-ray tube start angle. A similar dose optimization approach was adopted by Baader and colleagues for spiral CT body scans by varying the tube start angle, where an average dose reduction of 16 % was found compared to the mean value for the optimal start angle [8]. We are confident that the methods here set forth can be promptly extended to other anatomical regions of interest for HR-pQCT and validated by other researchers in their clinical radiological settings.

2. Materials and methods

We adopted digital twins of the scanned anatomy, available from previously acquired HR-pQCT (XtremeCT II, Scanco Medical AG, Brütisellen, Switzerland) bilateral scans of 10.4-mm thick sections of the tibia and radius of a 25-year-old female volunteer (176.6 cm body height, 78.3 kg body mass, body mass index 25.1, areal bone mineral density for L1–L3, 1.19 g/cm^2) [4]. These images were segmented via a semi-automatic dual-threshold algorithm (for details, see [4]) written in Fiji ImageJ image processing package [9] to identify the skin, soft tissue, muscle, bone, and yellow bone marrow (ybm) contained in the tomographic image. The segmentation of the bone used the thresholds recommended by the HR-pQCT guidelines (450 mg HA/cm^3 and 320 mg HA/cm^3 for the hydroxyapatite (HA)-calibrated cortical and trabecular bone densities, respectively) [1]. The output of the segmentation algorithm, representing a voxelized segmented phantom (with isotropic resolution of 120 μm for the absorbed dose simulations, and of 64 μm for the CT image reconstructions), is a digital twin of the real patient's anatomy. This is fed into our MC simulation code, which performs a virtual HR-pQCT scan of the patient via a digital twin representation of the Scanco second-generation scanner. We used a GPU-based MC software, gCTD [10,11], validated in previous work [4], to perform an *in-silico* HR-pQCT scan of the virtual patient. We set up a digital twin of the HR-pQCT scanner by reproducing the XtremeCT II X-ray spectrum

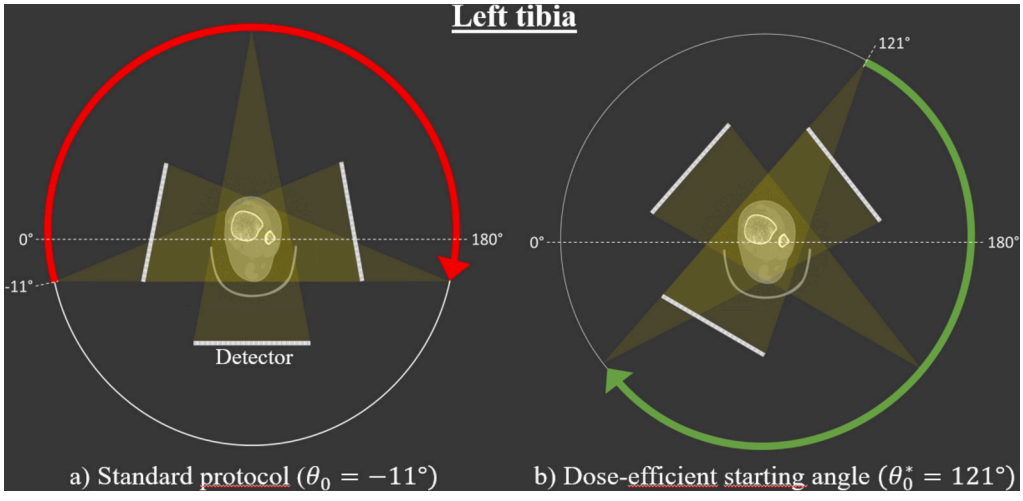

Fig. 1. Scheme of HR-pQCT bone scanning geometry for (a) the standard protocol (start angle $\theta_0 = -11^\circ$) and (b) a dose-optimized protocol (start angle θ_0^*). The half-scan angle (indicated by the curved arrows) is 180° + 22° fan angle, with 1011 projections equally spaced over 202° total scan angle. In the standard protocol, the scan angle covers the upper half-circle (from 0° to 180°) plus half fan angle (−11°, +11°) at the start and the end of the rotation. The ankle holder is positioned in the lower vertical half of the field of view.

(68 kV, filtration of 1 mm Al + 0.211 mm Cu + 0.3 mm Be) (reproduced using the web-based version of SpekPy ver. 2.0.8 [12]), focal spot (0.060 mm), scanning geometry (source-to-axis distance 400 mm, source-to-image distance 600 mm, partial scan angle 202°), and photon flux via CDTI calibration [4].

The MC simulation outputs an absorbed dose distribution in the voxelized phantom, as well as the dataset of CT projections from which a raw sinogram is produced, to obtain a digital HR-pQCT image of the patient's wrist or ankle, via cone-beam CT reconstruction. From the 3D absorbed dose map, we derived the average organ doses (for bone, muscle, fat, skin, and yellow bone marrow tissues), using a MATLAB R2024b script (The MathWorks, Inc., Natick, MA, USA). Lastly, the effective dose E (μSv) for the scan was computed from average organ doses, following the ICRP 103 report [13], the effective dose being "the risk-adjusted dosimetric quantity for the management of protection against stochastic effects" induced by radiation exposures.

For each of the four digital phantoms, we performed a single MC simulation with projections acquired over a full-orbit scan angle (360°) with an angular step of 0.2°. For every projection, the relative dose distribution map within the phantom was also saved to disk. We obtained the dose distribution for an HR-pQCT standard protocol scan by summing 1011 single-angle dose maps (900/180° views), starting from the angle $\theta_0 = -11^\circ$, over a half-scan angle (202°). We repeated this procedure for a varying start angle θ_0, in positive angular increments of $\Delta\theta_0 = 11^\circ$. For a full-scan simulation (360°), we then summed 1800 single-angle absorbed dose maps over 360°. Here, we report results for the half-scan angle procedure, with a varying start angle. Results for the full-scan angle are reported in the Supplementary material (Fig. S3), where a more homogeneous absorbed dose distribution can be observed in the 360° scan compared to the partial scan angle procedures. We evaluated the average organ dose and the effective dose as a function of the start angle θ_0. Details on the dose calculations can be found in [4].

For each of the four limbs examined, we analysed the dependence of the effective dose $E(\theta_0)$ on the tube start angle θ_0, and we determined the optimal start angle θ_0^* and the corresponding value $E^* = E(\theta_0^*)$. The optimal value was selected as the value of θ_0 for which E shows a minimum. The percentage dose reduction factor, ϵ_θ, was computed as follows:

$$\epsilon_\theta = 100 \cdot \frac{E(\theta_0) - E(\theta_0^*)}{E(\theta_0)} \quad (1)$$

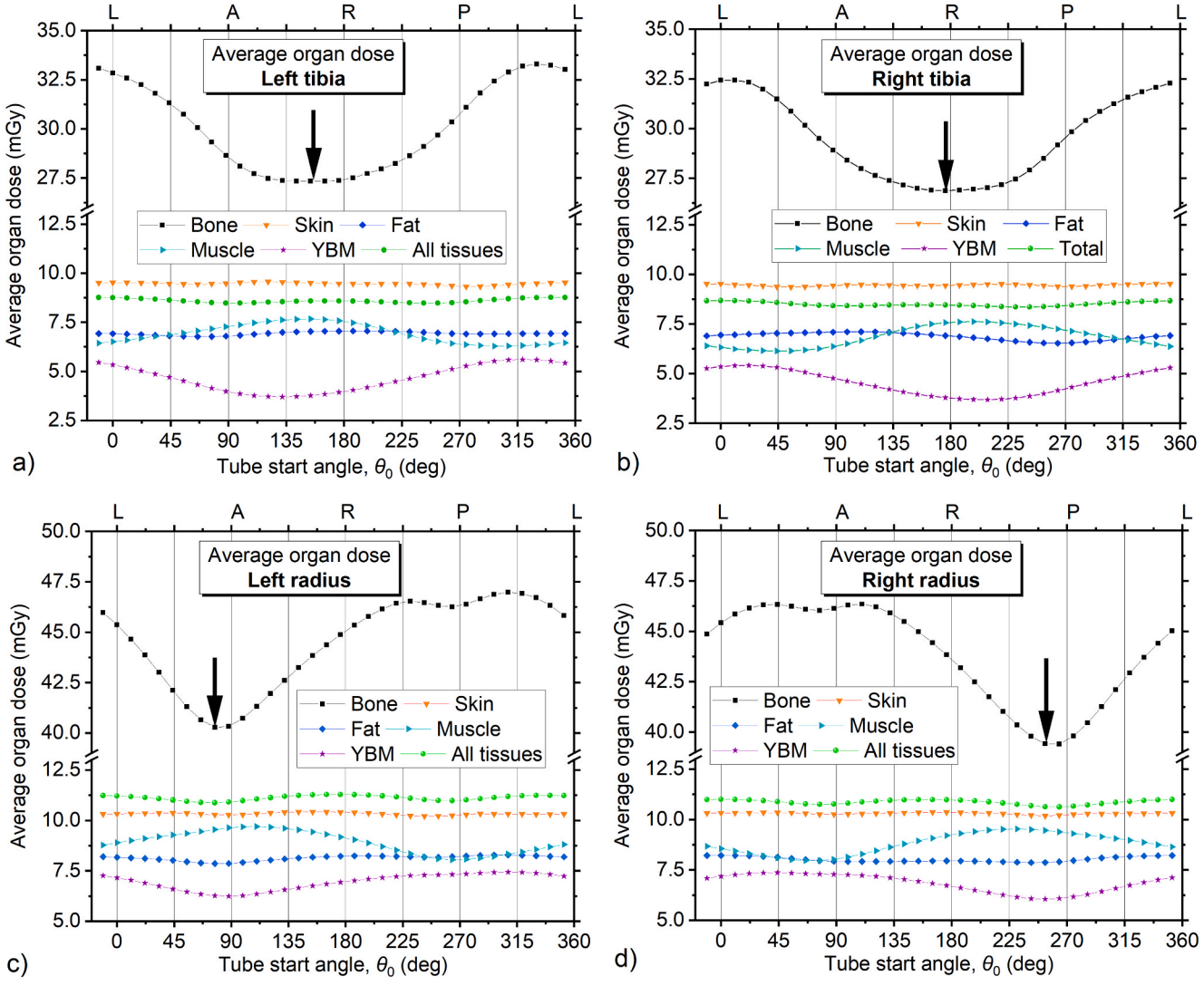

Fig. 2. Average organ dose (bone, skin, fat, muscle, ybm) as a function of the scan start angle θ_0 for the tibia left (a) and right (b); and for the radius left (c) and right (d). A symmetry between the left and right limbs can be found for both the tibia and radius. In all cases, the organ dose exhibits an absolute minimum (indicated by the arrow) for the bone (black squares) and ybm tissue (purple stars). The angular position of the X-ray tube is labelled L (lateral), A (anterior), R (right), P (posterior), with respect to the patient's view.

The effective dose we reported in the following does not account for the presence of the holder, as it was not included in our digital phantoms. Nevertheless, we explored its influence by including the carbon fiber holder in the digital phantom of the left tibia and simulating its irradiation. The holder material was simulated as carbon fiber with a composition of 95.5 % C, 2.5 % N, and 2 % O, and a density of 0.7 g/cm^3 [17]. We then repeated the effective dose calculation as described before.

We reconstructed CT images (2560 × 2560 × 160 voxels of 64 μm side) of the tibia from the simulated flat-field corrected projections, using the Python version of TIGRE [14]. An FDK reconstruction algorithm (Ram-Lak high-pass filter, no beam hardening correction) was used to obtain the 3D tomographic image of the object for the standard and dose-optimized protocols. Lastly, for an easier comparison, the dose-optimized image was rotated by 121° with respect to the orientation of the standard protocol.

3. Results

We obtained the 3D absorbed dose distribution within the voxelized digital phantoms, from which we determined the average organ dose. Fig. 2a shows the average organ dose as a function of the start angle θ_0, for the left tibia, for all tissues. The highest dose was absorbed in the bone, with a dose modulation as a function of the start angle, featuring a minimum dose at specific start angles θ_0. We observed a similar trend for the right tibia (Fig. 2b), with the angle of (absolute) minimum dose being different from the left side.

Fig. 2c and 2d show analogous plots for the two radii. We also assessed the uniformity of the dose distribution in each tissue (Fig. S2 in the Supplementary material). The absorbed dose maps for the radii are shown in Fig. S1 in the Supplementary material. The curves for the left and right radius are specular, both exhibiting a minimum for the bone dose (black line curve). Angular minima for bone dose are reported in Table 1.

Table 1
Angular minima(θ_0) for the absorbed doses in bone, ybm, skin and muscle, in the tibia and radius. The optimal start angle θ_0^* is also reported for both bones, based on the effective dose, calculated from the weighted mean of the dose contributions from different tissues. Therefore, the optimal start angle θ_0^* does not necessarily correspond to the minimum angle for any single tissue component. A range of ± 22° (i.e., $\Delta\theta_0$ used in the MC simulations) was assumed for the determination of θ_0^*, as the minima in *Evs*.θ_0 appear rather wide. An approximate relationship between θ_0^* for tibia and radius is found. The dose reduction factor reported in this table is calculated without the holder in place.

	Tibia		**Radius**	
Minimum angle	*Left*	*Right*	*Left*	*Right*
for bone dose	176°	165°	77°	264°
for bone marrow dose	209°	132°	88°	253°
for skin dose	55°	275°	242°	253°
for muscle dose	44°	297°	264°	66°
Optimal start angle, θ_0^* *for minimum E*	$\theta_{0,Left}^{*,Tibia}$ = 121° ±22°	$\theta_{0,Right}^{*,Tibia}$ = 220° ±22°	$\theta_{0,Left}^{*,Radius}$ = 77° ±22°	$\theta_{0,Right}^{*,Radius}$ = 264° ±22°
dose reduction factor,ϵ_θ	−9.9%	−10.4%	−5.8%	−6.6%
	$\theta_{0,Left}^{*,Tibia}$	$\theta_{0,Right}^{*,Tibia}$ @$\theta_{0,Left}^{*,Tibia}$ + 90°	$\theta_{0,Left}^{*,Radius}$	$\theta_{0,Right}^{*,Radius}$ @$\theta_{0,Left}^{*,Radius}$ + 180°

See Fig. 3 shows E calculated as a function of the start angle, for the right and left tibia (Fig. 3a) and for the left and right radius (Fig. 3b). E varies with θ_0 with a similar (oscillating) trend for both anatomical sides, showing an absolute minimum at specific start-angles θ_0^* (Table 1). The corresponding dose reduction (Eq. (1) is about $\epsilon_\theta = -10\%$ for the tibias and about $\epsilon_\theta = -6\%$ for the radii (Table 1). We note that the uncertainty we assigned to the optimal angle is ± 22° (full fan beam angle); In this range $(\theta_0^* \pm 22^\circ)$ the maximum percentage deviation of the effective dose from the absolute minimum 0.6 % in the interval $(\theta_0^* \pm 22^\circ)$. The statistical uncertainty in the above indicated ranges on the effective dose due to the Monte Carlo is 0.06 % (k = 3). Hence, the curve trend in the ± 22° interval is not dominated by the statistics but by the decrease in the dose across the minimum. We therefore believe that these considerations are sufficiently robust to support our indications for selecting the optimal starting angle.

As we found an "optimal" start angle determining a minimum for the effective dose, we analysed the corresponding 3D dose distribution and compared it to the one obtained for a standard protocol. Fig. 4 shows the dose map in the central slice of the left tibia for the standard scanning protocol (Fig. 4a) and the dose-efficient protocol (Fig. 4b). Here, we observed a dose gradient whose direction depends on the start angle. Fig. 4c,d show the same maps for the right tibia. CT reconstructions of image datasets for the standard and the dose-optimized protocols can be found in Figs. S4, S5, S6 of the Supplementary material. We quantified differences between the two reconstructions by analysing *i*) profiles across the trabecular structure, and *ii*) pixel value (attenuation coefficient) histograms of the two image datasets, in a region of interest selected within the trabecular region.

As reported in the supplementary material, pixel value volume histograms in the bone volume are substantially identical in terms of distribution moments, with minor differences due to the presence of streak artifacts. Moreover, a comparison between image line profiles (Figs. S4, S5, S6) showed a high morphological similarity between the two reconstructions.

We calculated the effect of including the carbon fiber limb holder in our optimized protocol. Indeed, any real scan of a patient with HR-pQCT is done with an holder to immobilize the limb. A virtual scan of the left tibia of the patient with the holder (Fig. S7) shows the following: (*i*) the effective dose still exhibits a minimum as a function of the tube starting angle; (ii) the optimal tube starting angle if the holder is considered, is shifted to higher values with respect to the optimal starting angle, θ_0^*, without the holder, but falls within the range (± 22°) we identified; (*iii*) due to the radiation shielding offered by the holder, the dose reduction factor ϵ_θ is − 16.6 %. This shows that, in real conditions, the achievable dose reduction factor can be even higher than calculated without considering the limb holder (− 9.9 %, Table 1).

4. Discussion

In the Scanco XtremeCT II HR-pQCT scanner, the technical setting of a standard protocol (e.g., as adopted at McCaig Institute for Bone and Joint Health, Calgary, Canada) adopts a fixed starting of the axial scan at $\theta_0 = -11^\circ$, with a half-scan angle of $\Delta\theta = 180^\circ + 22^\circ$ *fan angle* $= 202^\circ$ (Fig. 1a). This determines a marked non-homogeneous distribution of the absorbed dose in the irradiated tissues, as we observed in our previous study [4] (Fig. 2). Here we analysed, via MC simulations, the dependency of the organ dose and the effective dose on the start angle θ_0, which was varied from the standard value $\theta_0 = -11^\circ$ to $\theta_0 = 338^\circ$ in steps of half the fan angle ($\Delta\theta_0 = 11^\circ$). As shown in Fig. 3, there is a value of the start angle θ_0^* for which the effective dose for a tibia or radius scan exhibits a minimum. If the scan protocol selects a new start angle, $\theta_0 = \theta_0^*$, we expect that the corresponding dose burden to the patient can be reduced (by up to 10 % for the patient virtually examined in this work). The minimum of E vs θ_0 curve being relatively wide, we

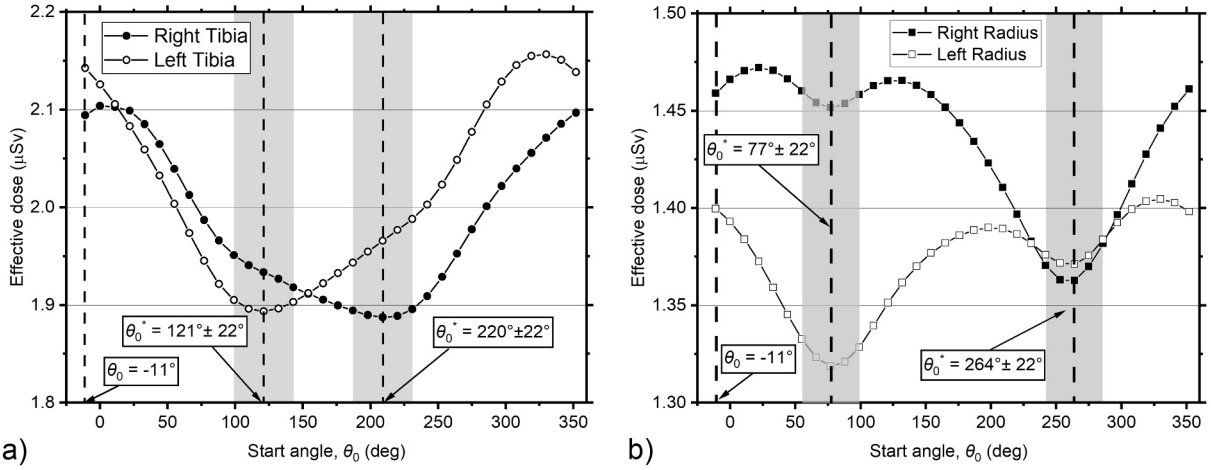

Fig. 3. Effective dose (μSv) per scan, $E(\theta_0)$, for the tibias (a) and radii (b), calculated at varying tube start angle, θ_0. An absolute minimum at the start angle θ_0^* is indicated on each plot, within a range of $\Delta\theta_0 = 11^\circ$. Vertical lines in the plot identify the minima for the effective dose; grey bands indicate a range of $\pm 11^\circ$ around the minima. The angular position of the X-ray tube is labelled L (lateral), A (anterior), R (right), P (posterior) with respect to the patient's view.

can assume that the range of selectable values for θ_0^* can be $\theta_0^* = 121^\circ \pm 22^\circ$ (Fig. 4b) and $\theta_0^* = 220^\circ \pm 22^\circ$ (Fig. 4d) for the left and right tibia, respectively.

Considering the anatomical symmetry between the left and right limbs, this permits us to suggest that an offset of about 90° exists between the two optimal angles θ_0^*. Hence, if the left tibia is scanned and an optimal start angle θ_0^* is found (via MC simulation), the optimal angle for the right limb could be assumed, as $\theta_0^* + 90^\circ$. For the radius, a reduction of up to 6.6 % can be achieved by selecting the start angle for the protocol. In this case, an offset of about 180° was found between the optimal angle for the left and right radius, suggesting a specular symmetry between the two limbs. Therefore, the possibility of selecting the optimal start angle for one limb knowing this parameter for the other one. Fig. 4 and Fig. S1 suggest that the optimal start angles can be understood with reference to anatomical symmetries (medial line between the bones), hence possibly putting the considerations here set forth on a firm basis.

We acknowledge that the first extensive demonstration of starting angle dose optimization was presented by Baader et al [8] in July 2024. However, we realized and suggested that such an optimization study could be performed for HR-pQCT in our previous paper [4] submitted in November 2024. Baader et al [8] paper (who also referred to previous studies from 2009 [15] and 2011 [16]) was dedicated to spiral CT, where the random tube starting angle is a relevant parameter for the helical scan, particularly in the beginning and end of the longitudinal scan. In the present work, we showed the non-trivial observation of the reduction of the effective dose in a fan beam CT (with no longitudinal movement) exam like HR-pQCT, for which the starting angle is fixed in the available commercial scanner, upon a suitable starting angular position. This circumstance was never explored in the available literature and therefore represents an element of novelty worth reporting in this proof-of-principle study.

A number of limitations affect the results of this study, namely *(i)* the cohort of the study being limited to one patient (two anatomical districts, bilateral scans); *(ii)* the related effect of anatomical variability among patients (body mass index, age, osteoporotic bone characteristics, and sex-related differences); *(iii)* we determined the influence of the limb holder in just a tibia scan, and we point out that the dose reduction factor can be different for a radius scan, as the holder's shape is completely different; (*iv*) a morphological analysis of the reconstructed images (e.g., trabecular bone volume fraction, trabecular thickness, and trabecular number) was not performed, as the proprietary Scanco software did not support this analysis for our datasets. However, we plan to evaluate the reconstructed images at the bone microarchitecture level in a future study to investigate whether the choice of the acquisition protocol influences these morphological parameters.

These limitations prevent us from concluding that the optimal angle found for this patient can be generalized to a large population. However, in this short report, we reported a complete analysis for one female patient to support a proof of principle for a dose reduction strategy in HR-pQCT with a minimal, easily implementable change to the standard protocol. Further studies on large cohorts will ascertain the general validity of the dose-optimized start angle setting in the population of HR-pQCT patients.

5. Conclusions

In this study, we found that a reduction of up to 10 % in the effective dose in an HR-pQCT examination can be achieved with the proper selection of the X-ray tube start angle. No significant impact on the reconstructed image was observed. Results suggest that the implementation of such a dose-optimized protocol in clinical practice could lead to a reduction in the patient's effective dose without negatively impacting the image quality. We believe that this work obeys to the ICRP recommendations on optimizing the radiation dose without detriment to the diagnostic value of the examination. While it is true that HR-pQCT dose is extremely low (less than 5 μSv according to the manufacturer and less than 2 μSv according to our simulation study presented in [4]), since the choice of the starting angle is, in principle, arbitrary, it is worth investigating the potentially beneficial effects of changing it, with the aim of delivering an as low as reasonably achievable dose to the patient. The described protocol for reducing patient dose could be readily implemented in a clinical setting as it only requires a change in the protocol's tube start angle. After acquiring a patient scan, the optimal scan angle is determined via a Monte Carlo simulation, and the corresponding optimal angle for the contralateral limb can then be inferred. This study did not include any clinical validation, but it only suggests a possible methodology for reducing the dose that should be evaluated in a prospective clinical setting. Future studies involving a larger patient cohort will enable the identification of optimal angles for each scan site and might validate the proposed optimized protocol, possibly leading to an update of current clinical protocols.

Data and software availability.

The MC simulation code gCTD is available upon reasonable request from Prof. Dr. Xun Jia (Johns Hopkins University). The dual-thresholding semi-automatic segmentation algorithm (written in Fiji) and the software for the effective dose computation (written in Matlab) are available upon reasonable request from Laura A. Cerbone

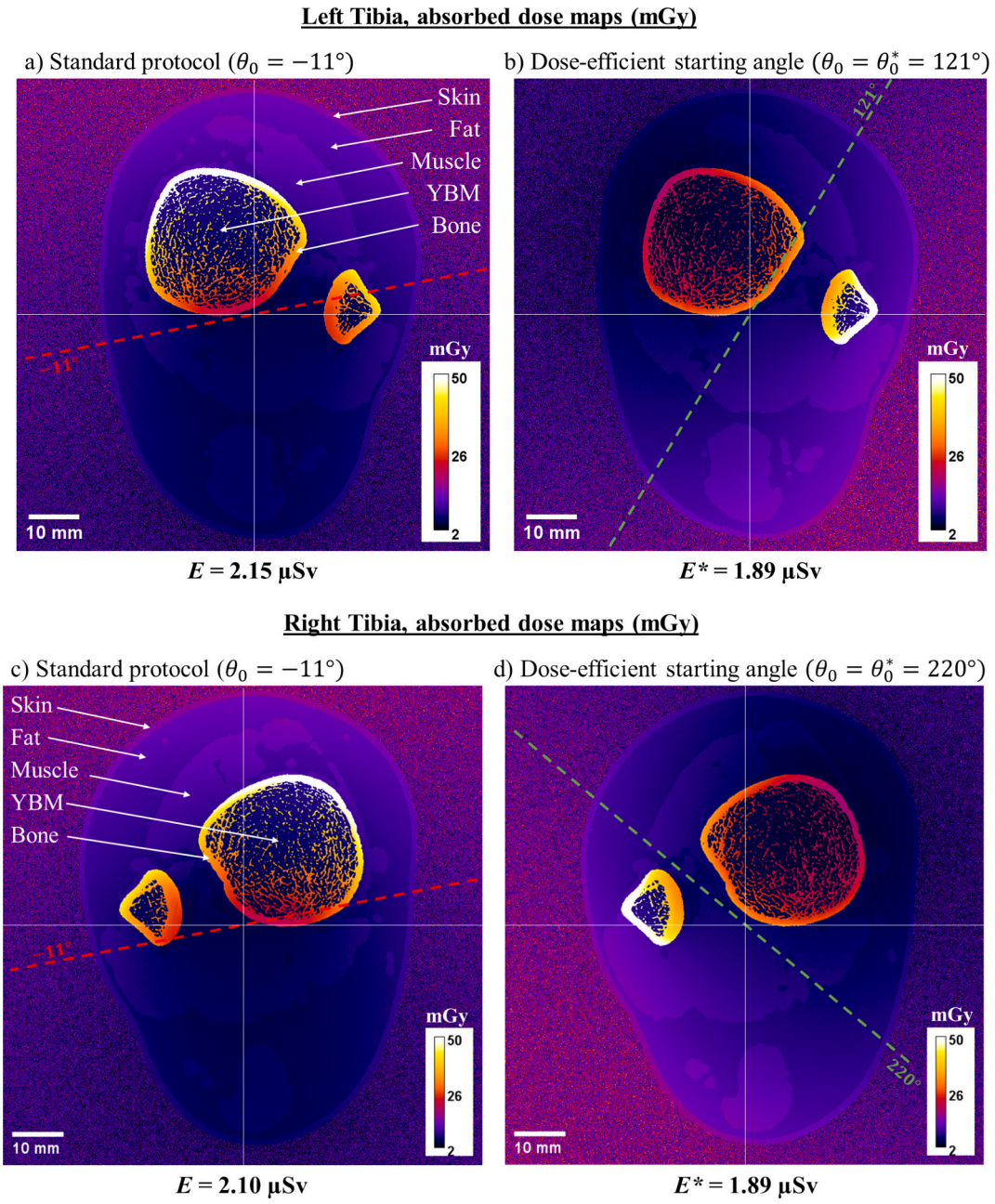

Fig. 4. Absorbed dose map (in mGy) in the central slice of the left (a, b) and right (c, d) tibias, for the standard scan protocol (a, c) and for the dose-optimized protocol (b, d). In each panel, the effective dose for the scan is indicated for the standard protocol (E) and for the scan at the optimal start angle $E^* = E(\theta_0^*)$. The dashed lines show the direction of c) the standard, and d) the dose-optimized tube start angle.

(Università di Napoli Federico II).

Ethical statement.

The HR-pQCT scan of a volunteer, used for this work in the form of a digital twin of the patient anatomy as available from a previous work, was originally approved by the University of Calgary Health Research Ethics Board within the Calgary Bone Health Study (CaBHS).

CRediT authorship contribution statement

Laura Antonia Cerbone: Writing – review & editing, Writing – original draft, Visualization, Validation, Software, Methodology, Investigation, Data curation, Conceptualization. **Youfang Lai:** Writing – review & editing, Software. **Xun Jia:** Writing – review & editing, Software. **Steven K. Boyd:** Writing – review & editing, Methodology. **Giovanni Mettivier:** Writing – review & editing, Software, Resources, Funding acquisition. **Paolo Russo:** Writing – review & editing, Writing – original draft, Visualization, Validation, Supervision, Project administration, Methodology, Investigation, Conceptualization.

Declaration of competing interest

The authors declare that they have no known competing financial interests or personal relationships that could have appeared to influence the work reported in this paper.

Acknowledgments

This work was carried out within the DXA4A (DXA scan for astronauts) project funded by Università di Napoli Federico II; it also contributes to the activities of the projects VITA and MEDIPIX4, funded by

INFN, Italy. The authors thank Noah R. Schafer (IEAP CTU, Prague, Czech Republic) for providing the CT reconstruction code based on the TIGRE CT reconstruction toolkit.

Appendix A. Supplementary data

Supplementary data to this article can be found online at https://doi.org/10.1016/j.ejrad.2026.113198.

Data availability

Data will be made available on request.

References

[1] D.E. Whittier, S.K. Boyd, A.J. Burghardt, J. Paccou, A. Ghasem-Zadeh, R. Chapurlat, K. Engelke, M.L. Bouxsein, Guidelines for the assessment of bone density and microarchitecture in vivo using high-resolution peripheral quantitative computed tomography, Osteoporos Int. 31 (9) (2020) 1607–1627, https://doi.org/10.1007/s00198-020-05438-5.

[2] S.L. Manske, Y. Zhu, C. Sandino, S.K. Boyd, Human trabecular bone microarchitecture can be assessed independently of density with second generation HR-pQCT, Bone 79 (2015) 213–221, https://doi.org/10.1016/j.bone.2015.06.006.

[3] K.K. Nishiyama, E. Shane, Clinical imaging of bone microarchitecture with HR-pQCT, Curr. Osteoporos. Rep. 11 (2) (2013) 147–155, https://doi.org/10.1007/s11914-013-0142-7.

[4] L.A. Cerbone, G. Mettivier, Y. Lai, X. Jia, S.K. Boyd, P. Russo, Absorbed and effective dose estimates in HR-pQCT of the distal radius and tibia: virtual dosimetry with a GPU-accelerated Monte Carlo code, Phys. Med. Biol. 70 (9) (2025) 095005, https://doi.org/10.1088/1361-6560/adc9f6.

[5] J. Damilakis, J.E. Adams, G. Guglielmi, T.M. Link, Radiation exposure in X-ray based imaging techniques in osteoporosis, Eur. Radiol. 20 (2010) 2707–2714, https://doi.org/10.1007/s00330-010-1845-0.

[6] W. Rühm, K. Applegate, N. Ban, F. Bochud, S. Bouffler, K.-W. Cho, C. Clement, E. Gallego, O. German, G. Hirth, Essentials of the system of radiological protection, J. Radiol. Prot. 45 (2025) 033002, https://doi.org/10.1088/1361-6498/ae02a2.

[7] M.M. Rehani, T.P. Szczykutowicz, H. Zaidi, CT is still not a low-dose imaging modality, Med. Phys. 47 (2) (2020) 293–296, https://doi.org/10.1002/mp.14000.

[8] E. Baader, L. Klein, J. Maier, S. Sawall, M. Kachelrieß, Patient radiation risk reduction by controlling the tube start angle in single and dual source spiral CT scans: a simulation study, Med. Phys. 51 (10) (2024) 7080–7092, https://doi.org/10.1002/mp.17290.

[9] J. Schindelin, I. Arganda-Carreras, E. Frise, V. Kaynig, M. Longair, T. Pietzsch, S. Preibisch, C. Rueden, S. Saalfeld, B. Schmid, J.-Y. Tinevez, D.J. White, V. Hartenstein, K. Eliceiri, P. Tomancak, A. Cardona, Fiji: an open-source platform for biological-image analysis, Nat. Methods 9 (7) (2012) 676–682, https://doi.org/10.1038/nmeth.2019.

[10] X. Jia, H. Yan, L. Cerviño, M. Folkerts, S.B. Jiang, A GPU tool for efficient, accurate, and realistic simulation of cone beam CT projections, Med. Phys. 39 (12) (2012) 7368–7378, https://doi.org/10.1118/1.4766436.

[11] X. Jia, H. Yan, X. Gu, S.B. Jiang, Fast Monte Carlo simulation for patient-specific CT/CBCT imaging dose calculation, Phys. Med. Biol. 57 (3) (2012) 577–590, https://doi.org/10.1088/0031-9155/57/3/577.

[12] G. Poludniowski, A. Omar, R. Bujila, P. Andreo, SpekPy v2.0-a software toolkit for modelling x-ray tube spectra, Med. Phys. 48 (7) (2021) 3630–3637, https://doi.org/10.1002/mp.14945.

[13] ICRP, 2007. The 2007 Recommendations of the International Commission on Radiological Protection. ICRP Publication 103. Ann. ICRP 2007;37:2-4. https://www.icrp.org/publication.asp?id=ICRP%20Publication%20103.

[14] A. Biguri, M. Dosanjh, S. Hancock, M. Soleimani, TIGRE: a MATLAB-GPU toolbox for CBCT image reconstruction, Biomed. Phys. Eng. Express 2 (5) (2016) 055010, https://doi.org/10.1088/2057-1976/2/5/055010.

[15] D. Zhang, M. Zankl, J.J. DeMarco, C.H. Cagnon, E. Angel, A.C. Turner, M. F. McNitt-Gray, Reducing radiation dose to selected organs by selecting the tube start angle in MDCT helical scans: a Monte Carlo based study, Med. Phys. 36 (2009) 5654–5664, https://doi.org/10.1118/1.3259773.

[16] Winslow, J.F., Tien C.J., Hintenlang D.E. Organ dose and inherent uncertainty in helical CT dosimetry due to quasiperiodic dose distributions. Med Phys. 2011;38 (6):3177-3185.8. Doi: 10.1118/1.3590367.

[17] A. Savini, F. Bartolucci, C. Fidanza, F. Rosica, G. Orlandi, Modeling of couch transmission in the RayStation treatment planning system, Phys. Med. 32 (2016) 735–740, https://doi.org/10.1016/j.ejmp.2016.04.012.